CORONAL MASS EJECTION ACTIVITY DURING SOLAR CYCLE 23

Nat Gopalswamy[1], Alejandro Lara[2], Seiji Yashiro[2], Steven Nunes[2], and Russell A. Howard[3]

[1]NASA Goddard Space Flight Center, Laboratory for Extraterrestrial Physics, Greenbelt, MD 20771, USA
[2]The Catholic University of America, Washington DC 20064, USA
[3]The Naval Research Laboratory, Washington DC 20375, USA

ABSTRACT

We studied the solar cycle variation of various properties of coronal mass ejections (CMEs), such as daily CME rate, mean and median speeds, and the latitude of solar sources for cycle 23 (1996-2002). We find that (1) there is an order of magnitude increase in CME rate from the solar minimum (0.5/day) to maximum (6/day), (2) the maximum rate is significantly higher than previous estimates, (3) the mean and median speeds of CMEs also increase from minimum to maximum by a factor of 2, (4) the number of metric type II bursts (summed over CR) tracks CME rate, but the CME speed seems to be only of secondary importance, (5) for type II bursts originating farther from the Sun the CME speed is important, (6) the latitude distribution of CMEs separate the prominence-associated (high-latitude) and active-region associated CMEs, and (7) the rate of high-latitude CMEs shows north-south asymmetry and the cessation eruptions in the north and south roughly mark the polarity reversals. We compared the rates of the fast-and-wide CMEs, major solar flares, interplanetary (IP) shocks, long-wavelength type II bursts and large SEP events. This comparison revealed that the number of major flares is generally too large compared to all the other numbers. In other words, fast-and-wide CMEs, long-wavelength type II bursts, large SEP events, and IP shocks have a close physical relationship.

Key words: CMEs; Solar Cycle Variations.

1. INTRODUCTION

Coronal mass ejections (CMEs) bring about large-scale changes in the corona, which have fundamental implications for the evolution of the magnetic-flux of the Sun, ultimately related to the solar dynamo (Low, 2001). Long-term behavior of the CME phenomenon was considered by a number of authors by piecing together data from different spacecraft (Webb and Howard, 1994; Cliver et al., 1994). The Solar and Heliospheric Observatory (SOHO) mission's Large Angle and Spectrometric Coronagraph (LASCO, Brueckner et al., 1995), images the corona continuously since 1996 covering a field of view starting from about 1.5 R_s to 32 R_s. This represents an unprecedented uniformity in data coverage from solar minimum to maximum and beyond with a single spacecraft. Combined with the availability of a large number of other spacecraft for measuring related eruptive phenomena, we have an excellent opportunity to study the long-term behavior of solar eruptions. In this paper, we present preliminary results on the variability of properties of CMEs with the progression of the current solar cycle (23). In particular, we consider CME rate and speed and how they relate to other tracers of solar activity cycle such as the sunspot number, type II radio bursts, prominence eruptions, and the tilt angle of the heliospheric current sheet. We also consider special populations of CMEs such as halo CMEs and high-energy CMEs (Gopalswamy et al., 2003c). The high-energy CMEs generally originate from active regions, which are important from the point of view of geoeffectiveness (Gopalswamy, 2002). Another special population is the high-latitude CMEs, which are expected to be related only to prominence eruptions, and hence are likely to be different from the CMEs originating from active regions.

2. SOLAR CYCLE VARIATION OF CME OCCURRENCE

The solar-minimum corona is characterized by the equatorial streamer belt, while the maximum corona has streamer structures all over the Sun. Figure 1 shows the solar corona during the minimum and maximum phases of the current solar cycle (23). The coronal structures essentially reflect the latitudinal excursions of the source-surface neutral line in the two phases. Since CMEs occur from closed magnetic field regions, one expects a corresponding change in the distribution of source regions. Figure 1 also shows the X-ray images of the corona underlying the white-light features. The distribution of the bright regions on the Sun again reflects the distribution of

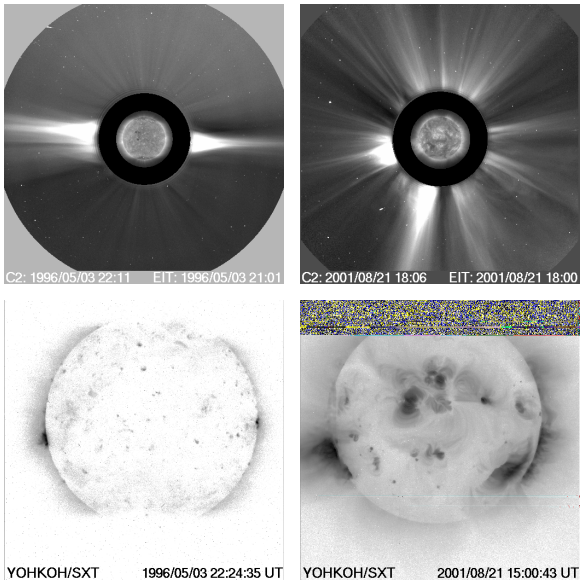

Figure 1. The outer and inner corona during solar minimum (left) and maximum (right) as observed by SOHO/LASCO (top) and Yohkoh mission's soft X-ray telescope (SXT) (bottom). The SXT image has its intensity reversed so the darkest regions have the highest intensity. The LASCO images have the SOHO/EIT images superposed to show features similar to those in the SXT images.

closed filed regions on the Sun, primarily belonging to one class, viz., active regions. Filament regions is another kind of closed field regions from which CMEs originate. The spatial distribution of filament and active region sources have different dependencies on the solar activity cycle and accordingly the associated CMEs are also expected to have different behavior with the solar cycle.

2.1. CME Rate

Tousey et al. (1974) used OSO-7 coronagraph data obtained over a 19.5 month period (November 1971 to May 1973) to estimate a rate of 14 CMEs per month (0.5 CMEs/day). OSO-7 had observed only 23 CMEs in all. Skylab observed 110 CMEs during its 227 days of observations, with which Hildner et al. (1976) estimated a rate of 30 CMEs per month (1 a day). Detailed investigation of CME rates by combining all the available data on CMEs from Skylab, SMM/CP, P78-1/Solwind was performed by Webb and Howard (1994) including correction for the visibility function. The long-term averaged CME rate obtained by them was in line with the prediction of Hildner et al. (1976). Averaging over much shorter time scales (over the Carrington Rotation period) Cliver et al (1994) obtained similar results. Based on the first two years of operation of SOHO, St. Cyr et al (2000) studied the CME rate and found them to increase steadily during the rise phase of the solar cycle. They concluded that the fundamental statistical measures of CMEs have not been significantly different from pre-SOHO observations. In this work we studied the CME rate from the minimum through the maximum activity phases of the current cycle (23).

The annual distributions of the widths and speeds of all CMEs from 1996 to 2002 are shown in Fig. 2. The number of CMEs observed in each year is shown on the width plot. The actual number of observed CMEs might differ substantially if there are data gaps. The major data gaps occurred in 1998 when SOHO mission was interrupted from June 24 to October 15 1998. There was also another gap of one month in January 1999. In spite of these gaps, we note that the number of CMEs per year is much larger than those reported by earlier coronagraphs at the corresponding phases of the previous solar cycles. The number of CMEs observed in 2002 alone (1637) is similar to the number of CMEs observed during the entire mission life time of SMM (1206) and P78-1 (1607) coronagraphs. The substantial increase in the number can be attributed to the increased sensitivity of the LASCO, which has a dynamic range of 6000, as compared to 40 and 30 for the SMM and P78-1 coronagraphs (see St. Cyr et al., 2000). The significantly larger field of view of LASCO also contributes to the higher number of CMEs detected. We also note several additional features in the annual distribution: The CME number drops from a high value of 1577 in year 2000 to 1463 in 2001 (7% drop) and then goes back up to the largest value (1637, a 12% increase) for cycle 23 in 2002. The numbers here have to be treated as lower limits because, the detection and measurements were made manually. Our inter-person calibration for test periods has shown that the error in the number of CMEs and the CME speeds is typically within 10%. The simple criterion employed in counting the CMEs is that an enhanced coronal feature should move in at least two consecutive frames of LASCO images. If a CME is obvious in a single frame, it is counted but it will not have speed. In the earlier study by St. Cyr et al. (2000) a criterion that the width of the moving feature should be $\geq 5^\circ$ was employed. Figure 2 shows that the 5-10° bin is the lowest bin to be populated. St. Cyr et al. (2000) had also set aside some events as 'anomaly' events, which we included as CMEs. This results in a slightly larger number of CMEs during the corresponding intervals.

The LASCO CME rate averaged over Carrington Rotation (CR) periods is given in Fig. 3. What is plotted is the observed CME rate (R_{obs}), which is simply the number of CMEs in a CR divided by the SOHO up-time (T_u, measured in days) during that CR. SOHO was not observing continuously, so the actual rate is expected to be different from the observed rate. Gopalswamy et al. (2003a) computed the upper limit to the CME rate on the basis of down times (T_d, measured in days) exceeding 3 h in each rotation period. If R_{max} is the maximum number of CMEs observed on any one day in a given CR, then assuming that CMEs occurred at R_{max} during T_d the upper limit to the rate was computed as $(T_u \times R_{obs} + T_d \times R_{max})/27.34$. The lower limit to

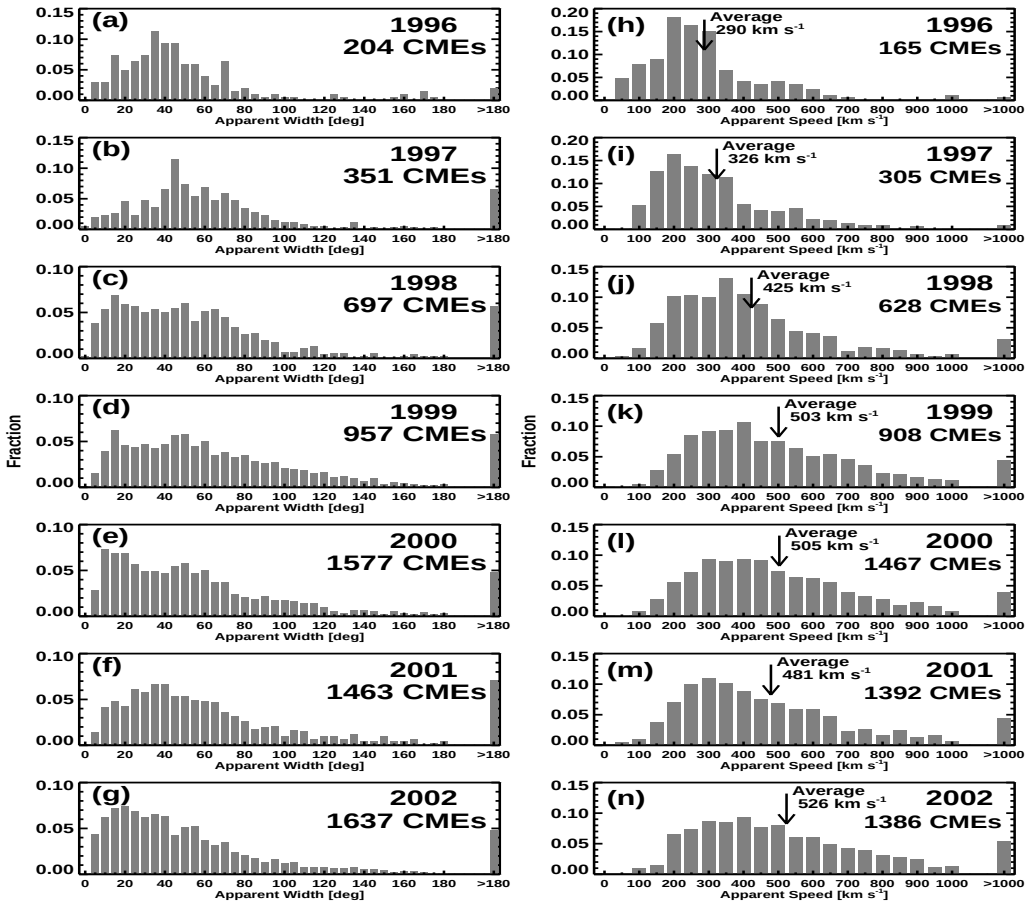

Figure 2. The width and speed distributions of SOHO/LASCO CMEs from 1996-2002. The number of CMEs detected in each year is given on the width plots. Speed could be measured only for a subset of all the detected CMEs, as shown on the speed plots. The last bin in the width plot includes all CMEs with width > 180°, which amounts to 2-7% of all the CMEs. The last bin in the speed plot includes all CMEs faster than 1000 km/s (up to 5% of all the CMEs). The annual averages (marked by arrows) clearly show increase in speed towards solar maximum.

the rate was obtained by assuming that the CMEs occurred at the observed rate during the down time: $R_{obs}/27.34$. Here we computed a simpler error bar assuming that the CME rate varies smoothly from rotation to rotation: the error bar for a given rotation is the product of $T_d/27.34$ and the average rate over three successive rotations (including the given rotation). These error bars are slightly smaller than the ones in Gopalswamy et al. (2003a).

Note that the CME rate increased from less than 1 during solar minimum in 1996 to slightly more than 6 in 2002. The rate during solar maximum is much higher than the highest corrected rate (3.11 per day) reported for previous cycles (Webb and Howard, 1994; Cliver et al., 1994). We have indicated the highest CME rates from previous coronagraphs and LASCO by the two horizontal dotted lines in Fig. 3. The highest LASCO rate (6.09) is almost twice as large as the SMM rate (3.11). Although the initial trend of CME rate over the first 2.5 years appeared to be consistent with the pre-SOHO rate, the LASCO rate turned out to be much higher during the maximum phase. The CME rate obviously has some cyclical behavior, which needs further investigation (see Ivanov and Obridko, 2001 for such behavior during previous cycles). It is possible that some head-on narrow CMEs may have been missed by LASCO, so a correction may be required as a visibility function (Webb and Howard, 1994). However, initial analysis by St. Cyr et al. (2000) suggests that such a correction may not be necessary for the LASCO data.

The days of the current solar cycle in which more than 10 CMEs occurred are shown in Table 1. The CR number in which these are contained and the average rates for these CRs are also given. There were 22 days between years 1999 and 2002 (1999 - 2, 2000 - 5, 2001 - 6, and 2002 - 9) that had more than 10 CMEs. Most of these days (73%) were in CRs that showed a local peak in the CR-averaged daily rate, including the two largest peaks of the cycle (CRs 1988 and 1993 with rates of 6.04 and 6.09, respectively).

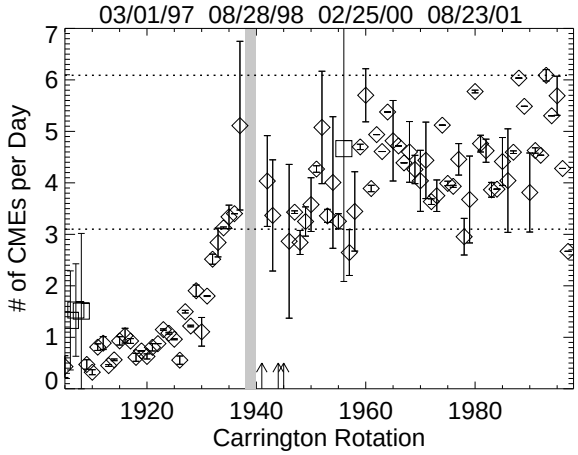

Figure 3. CME rate averaged over Carrington Rotation periods. The vertical shaded bar indicates the data gap due to SOHO mission interruption during June to October 1998. The three vertical arrows point to the three CRs during which observations were made only for less than 25% of the time and so the data points were dropped. The diamonds represent CRs with more than 75% data coverage. The squares represent CRs with only 50% data coverage. The horizontal dotted lines indicate the pre-SOHO (lower) and SOHO (upper) peak rates.

2.2. CME Rate and Sunspot Number

Based on the 110 Skylab CMEs, Hildner et al. (1976) found the CME rate (R) to be correlated with the sunspot number (N) and obtained the relation, R = 0.96+.084N (based on 7 rotations). They suggested that this relation is independent of the phase of the solar activity cycle and predicted a rate 3.2 per day (100 per month) for solar maxima. With new observations from Solwind and SMM/CP this relation was essentially confirmed (Webb and Howard, 1994; Cliver et al., 1994). SOHO/LASCO data also shows a good correlation (r=0.86), but the slope of the regression line is significantly different from the previous ones (see Fig. 4). We attribute this primarily to the better sensitivity of the LASCO coronagraphs and the enormous dynamic range. Additional factors include larger field of view and more uniform coverage over long periods of time. A surprising result of the comparison between CME rate and sunspot number is that the two did not peak at the same time. The peak CME rate for the current cycle occurred in 2002, well after the maximum of the sunspot cycle (in CR 1965, July 10-August 6, 2000). The CME rate peaked two years later (in CR 1993, August 8-September 9, 2002). In CR 1993 the Sunspot number was 128, much smaller than the maximum value.

From Fig. 4 it appears that the correlation between CME rate and Sunspot number is slightly weakened for higher (>90) sunspot numbers, beginning in 1999. Sunspots occur in active regions, so the correlation between CME rate and solar activity should be good only for those CMEs that originate from active regions. CMEs also originate from filament regions. It is well known that the phenomenon of rush to the poles starts before the maximum and disappears somewhere during the maximum. No sunspots are associated with the polar crown filaments, so the CMEs associated with the eruption of the PCFs have nothing to do with the sunspot activity. Therefore, we need to investigate the solar cycle variation of prominence eruptions and the CMEs associated with them.

Table 1. Days with 10 CMEs or more

		CMEs		
Date	CR	no.	Rate in CR	Peak?
1999/08/06	1952	10	5.08	Y
1999/09/17	1954	11	4.01	Y
2000/03/07	1960	11	5.70	Y
2000/07/16	1965	10	4.82	N
2000/10/04	1968	11	4.60	Y
2000/11/24	1970	11	4.04	N
2000/12/24	1971	11	4.44	Y
2001/03/07	1973	10	3.75	N
2001/03/08	1973	10	3.75	N
2001/03/21	1974	10	5.12	Y
2001/06/13	1977	12	4.46	Y
2001/06/18	1977	10	4.46	Y
2001/09/11	1980	11	5.77	Y
2002/01/30	1985	10	4.41	Y
2002/03/31	1988	13	6.04	Y
2002/04/14	1988	12	6.04	Y
2002/05/15	1989	10	5.49	N
2002/07/23	1992	10	4.54	N
2002/08/23	1993	11	6.09	Y
2002/10/25	1995	10	5.69	Y
2002/10/27	1995	13	5.69	Y
2002/10/29	1995	11	5.69	Y

2.3. CME Rate and Prominence Eruptions

The Nobeyama radioheliograph (NoRH) images the Sun in microwaves at 17 and 34 GHz for 8 h each day since 1992. Since prominences are cool ($\sim$ 8000 K), they are optically thick in microwaves and hence can be readily imaged (see, e.g. Gopalswamy, 1999). Recently, Gopalswamy et al. (2003b) studied the association between prominence eruptions detected automatically from the NoRH images and LASCO CMEs. They found that most of the filament eruptions were associated with CMEs. We extended that study to include the prominence eruptions in 2002. Fig. 5 shows the correlation between the prominence number in each CR and the number of CMEs in that rotation. There is clear correlation, but somewhat weaker than that between CME rate and sunspot number. This is expected because the majority of CMEs originate from active regions.

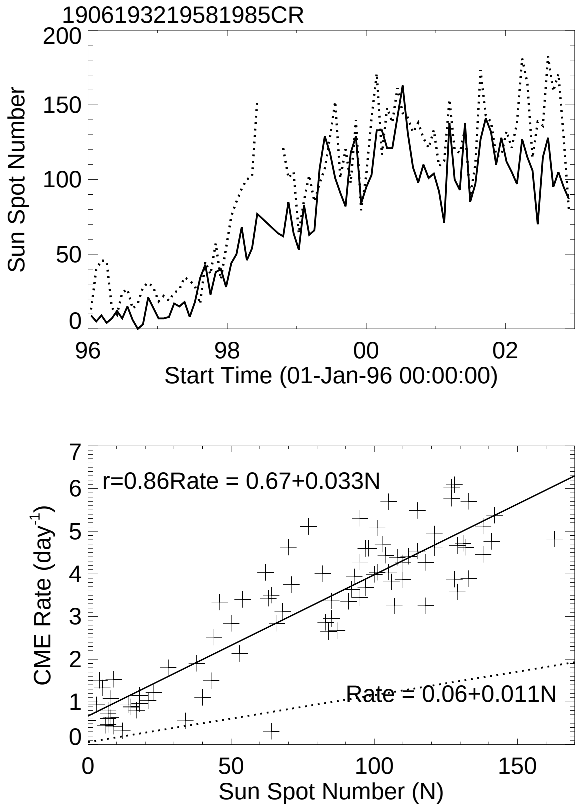

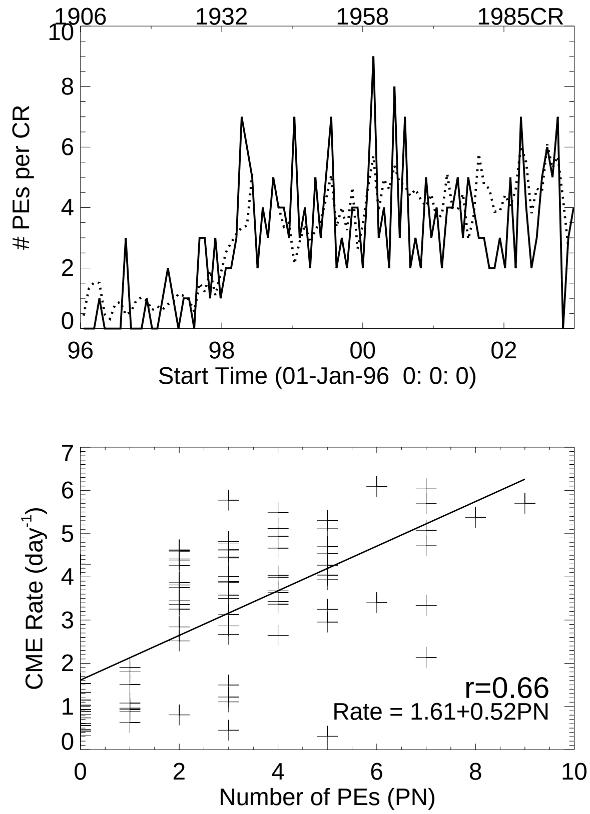

Figure 4(top)Comparison between CME rate and daily sunspot number (averaged over Carrington Rotation period) as a function of solar cycle. The Sun... ...sion line. The dotted line was obtained by Cliver et al. (199

Figure (top) Comparison between solar cycle variation of prominence eruption...

...ated with promi-
...n between CME rate and sunspot number, we have plotted the latitude of prominence eruptions and the associated CMEs as a function of ...

the known fact that the polarity reversal happens at the time of the disappearance of PCF (McIntosh, 2002; Lorenc... equatorward of the PCF. CMEs associated with the eruption of the PCF seem to facilitate this replacement. 1) the two poles had the same polarity. This means extremely ... between north and sou... weak to nonexistent global dipolar field. In fact, the tilt angle decreases su...

Most of the high-latitude CMEs are probably associated with the PCF. However, some CMEs originating from low latitudes may a... Thus, the central latitudes of CMEs can be used as an approximate discriminator between CMEs associated with PCF (lati... $> 60°$) and active regions (latitude $< 40°$). Figure 7 compares the CME rate for the high- and low-l... 1996...

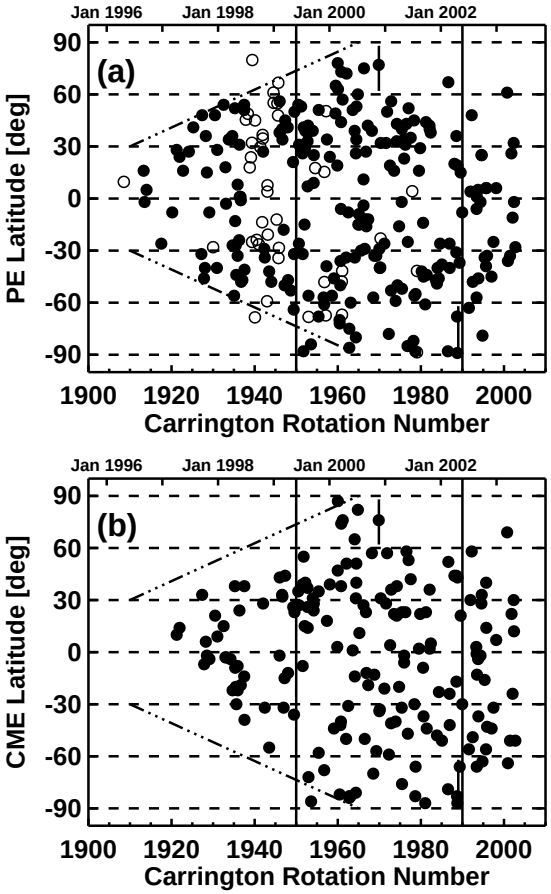

Figure 6. The latitude of CMEs (bottom) and prominence eruptions (top) as a function of time (both Carrington Rotation number and UT are given). The open circles in the PE plot indicate PEs that occurred during SOHO data gap. The slanted dot-dashed lines are drawn to guide the eyes to the spreading of eruptions to higher latitudes. The high-latitude eruptions occurred during the interval delineated by the two vertical lines. The short vertical lines mark the time of cessation of high latitude eruptions.

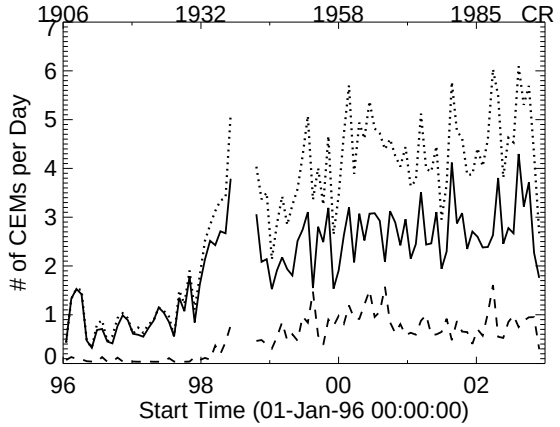

Figure 7. Comparison between low-latitude (solid line), high-latitude (dashed line) and total (dotted line) rates of CMEs as a function of time. Note that the low-latitude rate has a step-like behavior, which is modulated by the high-latitude rate.

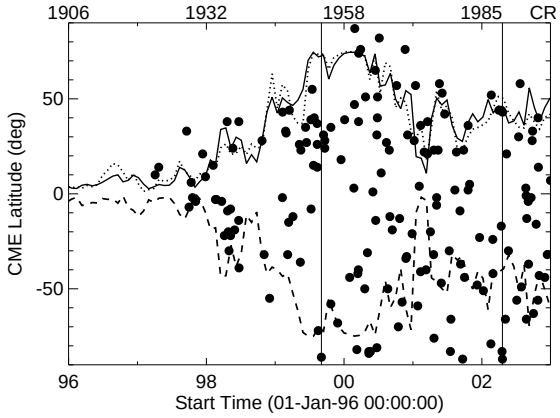

Figure 8. Latitudes of PE-related CMEs (filled circles) and the northern (dotted line) and southern (dashed line) maximum excursions of the heliospheric current sheet. The solid line represents the average of the northern and southern excursions. The vertical lines mark the start and end of high latitude CMEs.

initial jump in the year 1998, while the high-latitude CMEs show significant variations. For example, the steady decline in total rate in year 2000 is due entirely to the high-latitude CMEs. The spikes at the end of 2000 and at the beginning of 2002 mark the last spurt of activity at the time of polarity reversal. The 2002 spike, in fact, coincides with the second largest maximum rate for cycle 23 in March 2002.

2.4. Tilt Angle and CMEs

One way of looking at the spreading of CME and PE activities to higher latitudes is to examine the tilt angle (Cliver et al., 1994). The tilt angle is defined as the maximum extent of the heliospheric current sheet (HCS) and is computed by applying a potential field model to photospheric magnetic field observations (Hoeksema, 1992). Fig. 8 shows the maximum northern and southern extent and the average value of the HCS tilt angle with the locations of the CMEs associated with PEs superposed. We see that the tilt angle curve serves as a rough envelope of CME latitudes. The deviations during solar maximum may not be significant because the tilt angles above 70° are lower limits. The sharp decline in tilt angle in the beginning of year 2001 clearly has corresponding shift in the CME latitudes.

The CME rate and the magnitude of the tilt angle are compared as a function of time in Fig. 9. Following Cliver et al. (1994), we considered the 50° tilt angle to be a critical value, which roughly separates the minimum and maximum conditions. We can identify three intervals based on the value of the tilt angle: (i) the increasing phase from 1996 to middle of 1999 when the tilt angle increased from low values to about 50°, (ii) the maximum phase from middle 1999

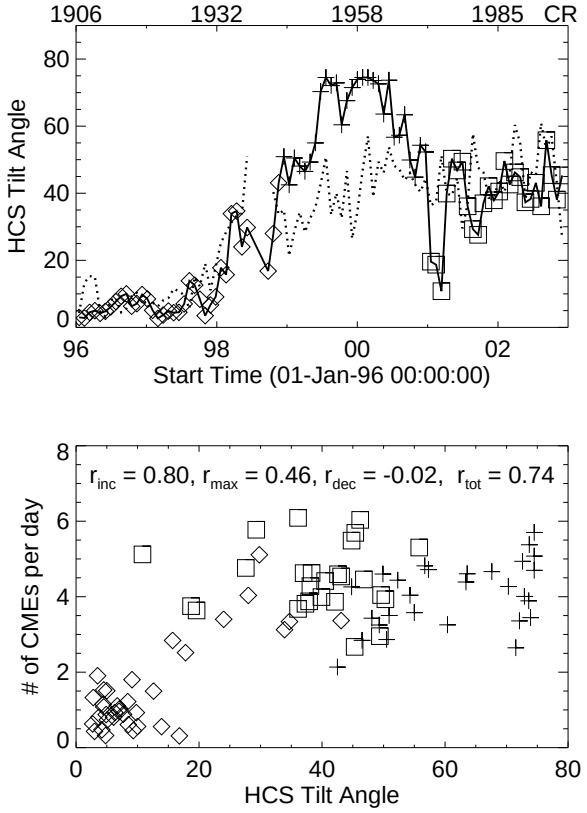

Figure 9. (top) Comparison between tilt angle of the heliospheric current sheet (solid line) and the daily CME rate (dotted line). The diamond, plus and square symbols denote periods when the tilt angle approached 50°, stayed above 50°, and declined to values below 50°, respectively. (bottom) Correlation between tilt angle of the heliospheric current sheet and CME rate. The rise phase has maximum correlation. The maximum and declining phases have much weaker correlation.

to beginning of 2001 when the tilt angle remained above 50° and (iii) the declining phase starting in early 2001, when the tilt angle dropped below 50°. While there is an overall correlation between CME rate and tilt angle (correlation coefficient r_{tot}=0.74), there are large deviations. The correlation is rather good for the increasing phase (r_{inc} = 0.80). During the maximum and declining phases the correlation is rather weak (r_{max} = 0.46, and r_{dec} = −0.02, for the maximum and declining phases, respectively).

3. VARIABILITY OF CME SPEED

Early compilation of the Solwind CME speeds indicated that the mean CME speeds increased towards solar maximum, although the SMM data did not indicate such a variation. In fact, Hundhausen (1999) remarked that the "speeds vary widely, even when averaged over intervals as long as a year." In Fig. 10 we have plotted the annual averages of CME speeds obtained by the Sol-

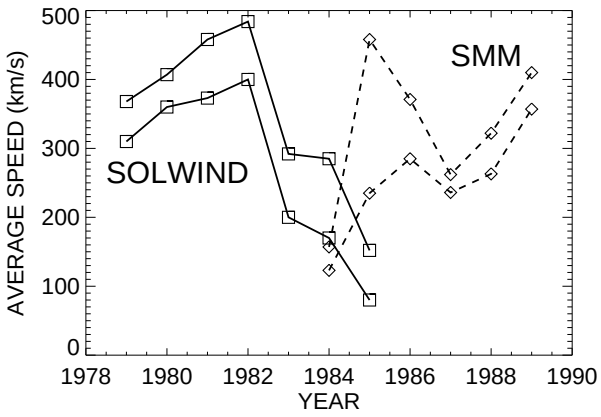

Figure 10. Annual averages of CME speeds from SMM and P78-1 spacecraft showing increase in speed towards solar maximum.

wind and SMM coronagraphs. The speed values were taken from St. Cyr et al. (1999) for 1980 to 1989. For the year 1979, we computed the average speed from the Solwind CME catalog (http://lasco-www.nrl.navy.mil/solwind_transient.list). Notice that both Solwind and SMM data points show a higher value for the maximum. The mean speed obtained from the SMM data for year 1985 is abnormally high in contrast to the Solwind value. Examination of the SMM CME catalog (Burkepile and St. Cyr, 1993) revealed that it was not possible to measure the speed of more than 40% of the CMEs (only 39 of the 62 CMEs had speeds). The SMM speed in 1985 (458 km/s) was the highest annual average from the entire SMM epoch (Hundhausen, 1999). On the contrary, Solwind detected the same number of CMEs (over a different time period in 1985) that resulted in a mean speed of only 150 km/s. The median speed, however, had a smaller variation. By combining the SMM and Solwind data, Ivanov and Obridko (2001) found that the semiannual averages of mean speed showed a peak near minimum (in the year 1985), in addition to the peaks in the maximum epochs (1981-1982, 1989).

Figure 11 shows the variability of the mean and median speeds of LASCO CMEs (annual and semi-annual averages). The annual average of the speed peaks in 2002, after the Sunspot maximum. Figure 12 shows the variability of the mean speed of LASCO CMEs averaged over CRs. There is a clear increase in the mean speed from the minimum to maximum by a factor of 2 (from 250 to 500 km/s). One of the largest peaks occurred in April 1998, when AR 8210 produced a large number of fast CMEs. These large peaks are associated with energetic eruptions accompanied by type II radio bursts and solar energetic particle (SEP) events.

Type II radio bursts are thought to be due to fast mode MHD shocks propagating through the corona and IP medium. The close association between type II bursts and CMEs suggests that the shocks are

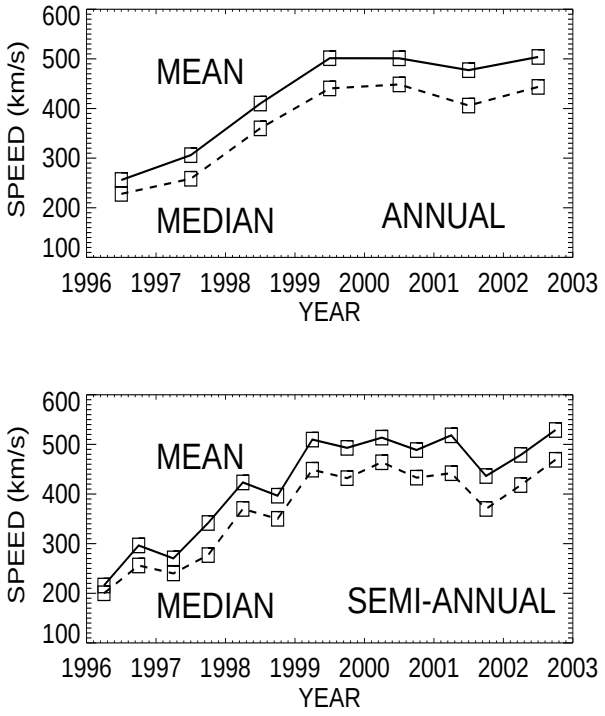

Figure 11. Annual and semiannual average speeds of LASCO CMEs.

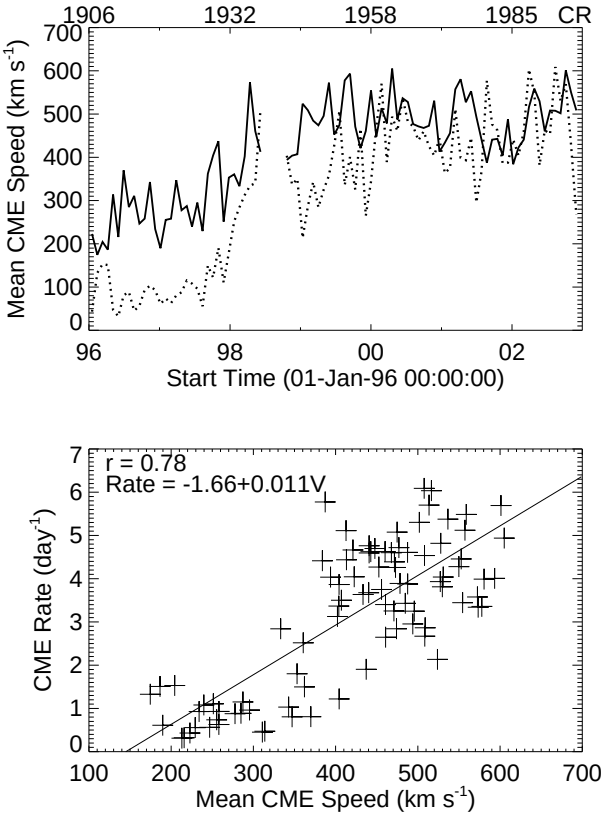

Figure 12. (top) CME mean speed (V) averaged over CRs (solid line) compared with daily CME rate (dotted line). (bottom) Correlation between CME rate and CME mean speed along with the regression line.

driven by CMEs and accelerate nonthermal electrons, which in turn produce radio emission via plasma processes. This scenario is confirmed by in situ observations of CME-driven shocks. The energy of the CME and the Alfven speed profile in the corona seem to be crucial factors in deciding whether the type II burst is associated with a CME (Gopalswamy et al., 2001a,b). There is a hierarchy of CME properties (speed, width, and acceleration) that can be associated with metric and decameter-hectometric (DH) type II bursts (Lara et al., 2003). Metric type II bursts correspond to shocks in the inner corona, while DH and longer wavelength type II bursts are indicative of shocks propagating from the Sun far into the IP medium. Figure 13 compares the CME rate with the number of type II bursts in the metric and DH domains. The overall correlation with the CME rate is stronger for the metric type II bursts than for the DH type II bursts. Most of the peaks in CME rate have corresponding peaks in the number of metric type II bursts. Note, however, that the number of metric type II bursts is typically an order of magnitude smaller than the number of CMEs in a given CR. For DH type II bursts, the CME has to be fast and wide (Gopalswamy et al., 2001b). In order to show this, we have plotted the CME mean speed variation along with the CME rate and DH type II number (summed over each CR) in Fig. 13. Note that there are several rotations throughout the solar cycle with no DH type II bursts. For most of these rotations, the CME mean speed has a local minimum, thus confirming the importance of CME speed in producing DH type II bursts.

4. SPECIAL POPULATIONS OF CMES AND THEIR SOLAR CYCLE VARIATION

Although nearly 7000 CMEs occurred during the first 7 years of the current solar cycle (23), only a small fraction (1-2%) of these CMEs are geoeffective. A CME is considered to be geoeffective if it produces an observable effect in the vicinity of Earth. For example, large geomagnetic storms are caused by CMEs impinging upon Earth. CMEs resulting in a significant enhancement of SEP intensity in geospace are also considered geoeffective. Although there is considerable overlap in the properties of the storm- and SEP-associated CMEs, there are some crucial differences in terms of their solar sources. The storm-causing CMEs need to be directed toward Earth and their magnetic structure must contain a southward component. On the other hand, the SEP-causing CMEs need to drive a shock that accelerate particles, which means they need to be fast and wide and the shocks need to cross the Sun-Earth flux tubes.

4.1. Halo CMEs

Halo CMEs are so named because they appear to surround the occulting disk of the coronagraph

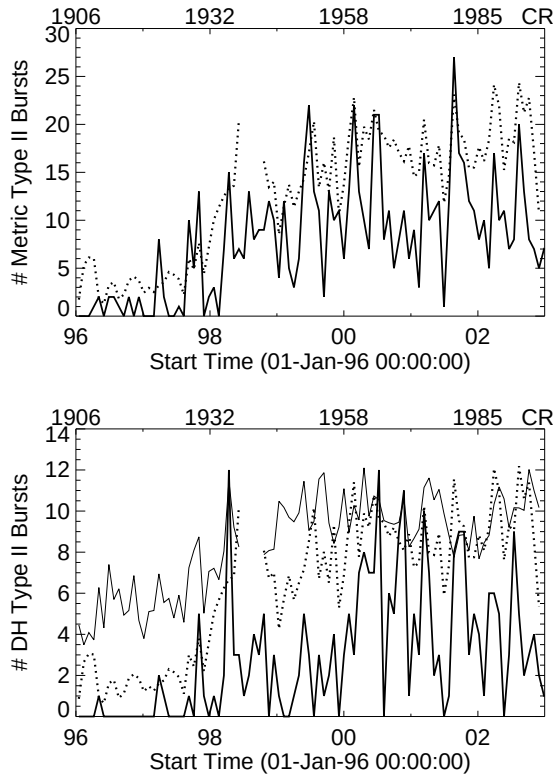

Figure 13. Daily CME rate (dotted line) compared with the number of metric type II bursts per CR (top - solid line) and DH type II bursts (bottom - solid line). The CME rate is multiplied by a factor of 4 (top) and 2 (bottom) to fit the scale. In the bottom panel, the mean speed (averaged over CR) is shown by thin lines.

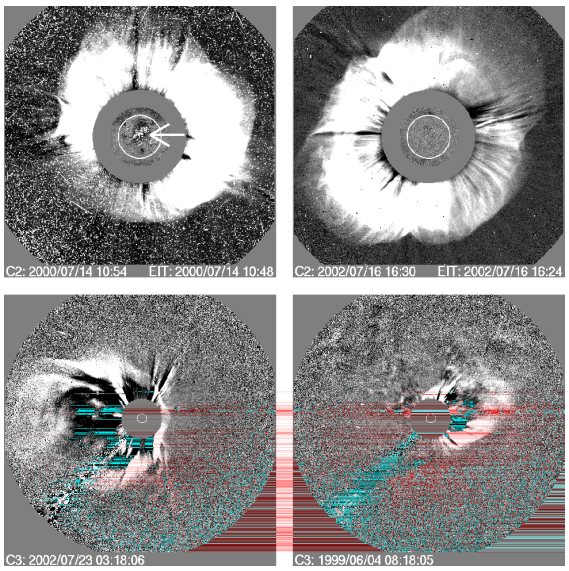

Figure 14. Examples of halo CMEs from SOHO/LASCO. The top two are C2 difference images of front-side (left) and back-side (right) full halos. The arrow points to the EUV eruption seen in the SOHO/EIT difference image superposed on the front-side halo image; no EUV activity is expected for the backside halo. Asymmetric halo (bottom left) and partial halo (bottom right) are shown from C3 difference images.

(Howard et al., 1982). CMEs directed both toward and away from Earth will appear as halo CMEs, but only the former will be geoeffective. Coronagraph images alone will not be able to distinguish between the front and backside halos, so one would need images of the disk in wavelengths such as EUV or soft X-rays. Fig. 14 shows two full halo CMEs one front-sided (with a clear activity in the EIT difference image) and the other back-sided (no activity seen in the EUV difference image). The front-sided event is the well-known Bastille day event (July 14, 2000). CMEs aimed off center from the Sun center can also appear as halos, but will appear asymmetric with respect to the occulting disk. CMEs aimed orthogonal to the Sun-Earth line may never appear to surround the occulting disk. Based on their appearance, halo CMEs can be classified as follows (see Fig. 14):

Full halos (type F): These are the classical halo CMEs, which appear to surround the occulting disk. Generally they originate from close to the disk center (frontside halo) or too far behind the limb (backside halo).

Asymmetric halos (type A): These are wide, near-limb CMEs, which become halos late in the event. For example, the CME does not appear to encircle the occulting disk in the C2 field of view (FOV). But by the time they expand to C3 FOV, they often have a faint extension above the opposite limb, thus giving the appearance of a full halo. The extension seen on the opposite limb may be the associated pressure wave or shock (see e.g. Sheeley et al., 2000).

Partial halos (type P): These are CMEs with width greater than 120° and never appear to completely surround the occulting disk.

Although halo CMEs had been known from pre-SOHO observations the LASCO instruments have demonstrated their prevalence (Webb et al., 2000; St. Cyr et al., 2000; Webb, 2002). Interplanetary ejecta (also known as interplanetary CMEs) seem to evolve out of Earth-directed CMEs (Gopalswamy et al., 2000), but the exact relationship between the near-Sun and near-Earth manifestations is not clear (see Gopalswamy, 2003 for a tentative correspondence). Initial indications were that the majority (80%) of intense (Kp $\geq$ 6) geomagnetic storms could be related to front-side halo CMEs (St. Cyr et al. 2000). Webb (2002) finds that the fraction of halos associated with geomagnetic storms considerably decreased towards solar maximum. For example, 92% of the halos were associated with geomagnetic storms in the year 1997, while the fraction dropped to 35% in the year 2000. This may be due to a combination of changes that take place during solar maximum: the IP medium is complex with interacting magnetic structures, the fraction of Earth-directed CMEs may be smaller due to the spreading of eruptions to higher

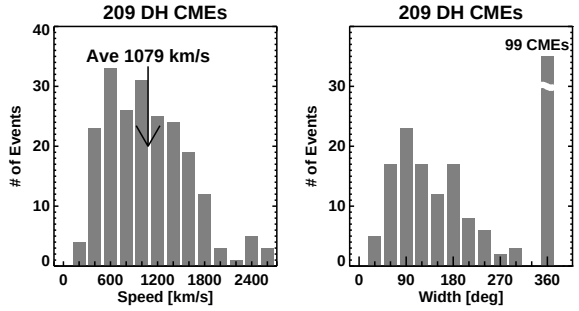

Figure 15. Speed (left) and width (right) of 209 CMEs associated with DH type II bursts (1996-2002). The average values of the distributions are given on the plots. Note that nearly half of the CMEs were halos.

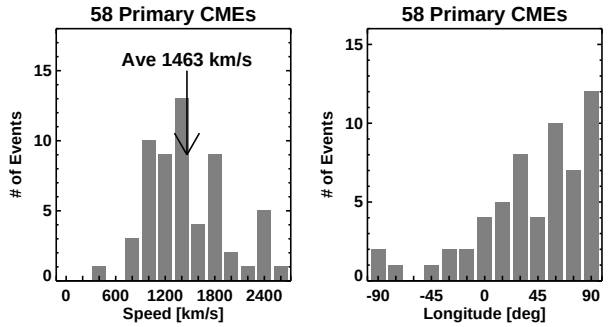

Figure 16. Speed (left) and source longitudes of 58 CMEs associated with major SEP events (1996-2002). Note that most of the SEP-associated CMEs originated from the western hemisphere.

latitudes, the change in sign of the solar dipolar field (which should have the same orientation as the leading fields in CMEs - see Crooker et al., 2000), and so on.

4.2. Fast and Wide CMEs

While many slow halo CMEs are known to cause geomagnetic storms, only fast and wide CMEs cause large energetic particle events (Gopalswamy et al., 2003c). Fast but narrow CMEs do not seem to accelerate electrons or ions (Gopalswamy et al., 2001b). For example, the speeds and widths of the CMEs associated with DH type II bursts are much larger than these of average CMEs (see Fig. 15). CMEs associated with SEPs are even faster (see Gopalswamy et al., 2002). Figure 16 shows that the CMEs associated with SEPs are fast (> 900 km/s) and wide ($> 60°$) and generally come from the western hemisphere. While it is not uncommon that CMEs from the eastern hemisphere are associated with SEP events at Earth, western hemispheric fast and wide CMEs result in prompt increase of SEP intensity at 1 AU.

The annual totals of the special populations are shown in Fig. 17. The halo CME rate peaked in year 2000, while the fast and wide CME rate peaked in 2002 similar to that of the general population. The

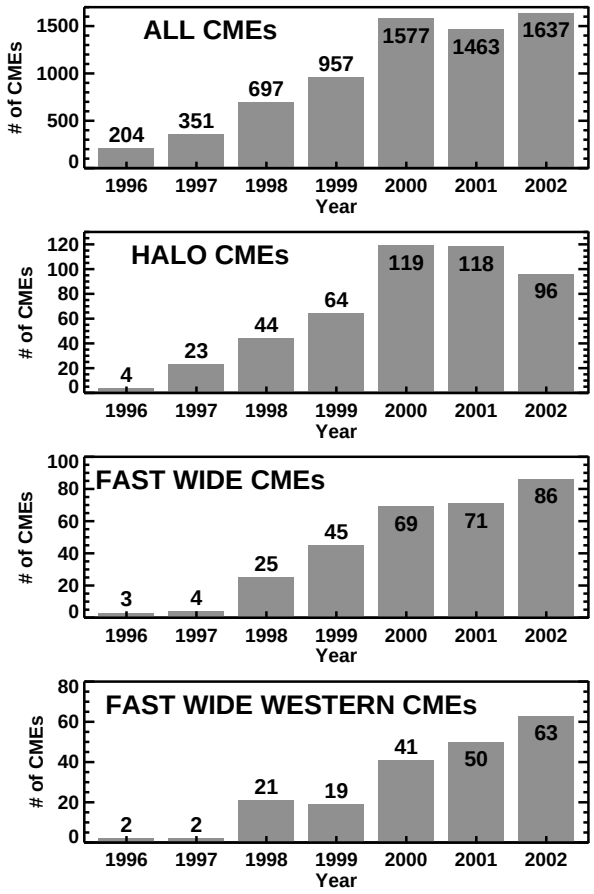

Figure 17. Annual numbers of the general and special populations of CMEs (halos, fast and wide, and fast-and-wide western CMEs). Halo CMEs include all CMEs with width = 360° (type F + type A) and those with width $>$ 180°. Fast and wide CMEs have speed > 900 km/s and width $> 60°$. Fast and wide western CMEs are the same as fast and wide CMEs, but their span includes position angle 270°. The numbers in each bin are marked. Note that the special populations are small fractions of the general population.

fast and wide western hemispheric CMEs is a subset of the fast and wide CMEs closely associated with SEPs. For the solar maximum phase (years 2000-2002), the number of halo CMEs exceeded 100 per year. Of these, only the Earth-directed ones need to be considered for geoeffectiveness. In the year 1999, the number of fast and wide western hemispheric CMEs is relatively small, consistent with the paucity of major SEP events in that year (Gopalswamy et al., 2003c).

Fig. 18 shows the solar cycle variation of the fast and wide CMEs and the related energetic events such as DH type II bursts, major SEP events (> 10 MeV protons from GOES), IP shocks (detected in situ) and major solar flares (M- and X-class only). The numbers plotted are the number of events binned into Carrington Rotations. The DH type II bursts (1-14 MHz) detected by the Wind/WAVES experiment have an excellent correlation with fast and

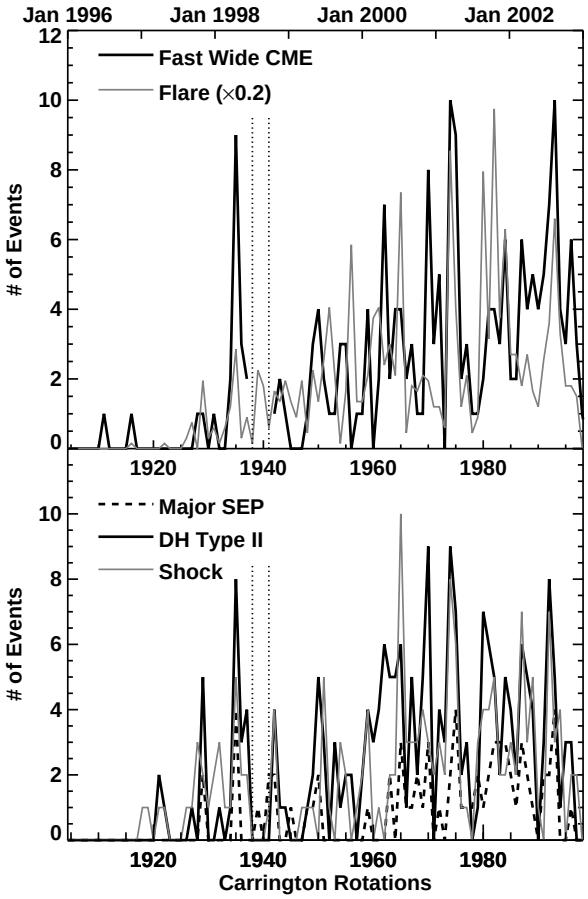

Figure 18. (top) Solar-cycle variation of the number of fast-and-wide CMEs and major (M and X) flares. (bottom) Solar-cycle variation of the number of major SEPs, DH type II bursts and interplanetary shocks. All the numbers are binned into Carrington Rotations. The number of flares is multiplied by 0.2 to fit within the scale. Note that the flare number is generally much larger than the rest and shows the maximum differences with other numbers. The vertical dotted lines mark the SOHO data gap.

wide CMEs and major SEP events. All have similar solar-cycle variation. Overall good close correlation implies physical relationship: the same CME-driven shock accelerates electrons that produce DH type II bursts, and SEPs. Note that the number of flares is divided by 5 to fit them within the scale. This means the number of flares is generally too large compared to the other numbers plotted. Even though the overall solar cycle variation is evident, some rotations (such as CR 1935 due to the super-active region 8210) are rich with energetic activity, while others were poor even during the solar maximum phase (CRs 1978 and 1979).

5. DISCUSSION AND CONCLUSIONS

The superior capability of the SOHO/LASCO coronagraph enabled us to observe CMEs with unprecedented continuity and spatial coverage and hence we have a better picture of the whole phenomenon from the minimum to post-maximum phases of solar cycle 23. There are several surprising results that came out of the study of nearly 7000 CMEs over a period of 7 years (1996-2002). The solar maximum rate was found to be much higher than previously thought. Even though there is good correlation between CME rate and Sunspot number, the peaks were nearly two years apart. The mean speed of the CMEs also shows a clear solar cycle variation, which nearly doubled from the minimum to maximum phases. By isolating the high latitude CMEs on the basis of prominence eruptions, we were able to show that they are intimately related to the polarity reversal during solar maximum. The cessation of high-latitude activity seem to clearly mark the completion of polarity reversals and that this process occurs in an asymmetric fashion at least for cycle 23. This leads to an important conclusion that the polarity reversal is an energetic process involving the release of large amounts of energy. The present study also points to the importance of the two classes of CMEs, which received attention for many different reasons. The high-latitude CMEs are clearly related to prominences and the low-latitude CMEs could be associated with both filaments and flares. The low-latitude CMEs are somewhat mixed because there are quiescent and active prominences at low latitudes. Grouping the CMEs into two classes may be more important than thought before from the point of view of how closed and open field structures evolve on the Sun over the solar cycle. The rate of high latitude CMEs is clearly related to the migration of closed field structures to the poles (one indication is the rush to the poles of the polar crown filaments, see Cliver et al., 1994) as signified by the high tilt angles. At the same time, the low-latitude CME rate seems to be rather flat at a higher rate. Occasionally the high-latitude rate can be as high as the low -latitude rate, but overall the low-latitude activity dominates. The separation also helped us have a better understanding of the solar cycle variation of CME rates because both sunspot activity and high latitude CME activity are high during solar maximum. Thus a high correlation between CME rate and sunspot number alone does not give a correct picture of the solar cycle variation of the CME phenomenon.

Halo CMEs and fast-and-wide CMEs constitute two special populations of CMEs that are important from the space weather point of view. Fortunately, these CMEs form a small subset and can be studied independent of the thousands of ordinary CMEs. The shock-driving capability of the fast and wide CMEs is an important aspect consistent with the current paradigm that energetic particles (in large events) are accelerated by these shocks. The solar cycle variation of these special populations is similar to the general population, but there can be large deviations owing to large-scale magnetic patterns present on the Sun.

ACKNOWLEDGMENTS

We thank all the members of the LASCO consortium (Naval Research Laboratory, USA; University of Birmingham, UK; Laboratoire d'Astronomie Spatiale, France; and Max-Planck-Institut fur Aeronomie, Germany) who built the coronagraphs and acquired the data used in this work. The preliminary SOHO/LASCO CME list developed by O. C. St. Cyr, S. P. Plunkett, and G. Lawrence have been very useful for further measurements. We thank N. B. Rich for formating the data suitable for measurements. G. Michalek and A. Rosas helped with CME height-time measurements. We thank K. Shibasaki for Nobeyama prominence data, T. Hoeksema (Wilcox Solar Observatory) for computed tilt angle data, M. L. Kaiser and J.-L. Bougeret for Wind/WAVES data, and D. Berdichevsky for shock data. SOHO is a project of international cooperation between ESA and NASA. This research was supported by NASA/LWS and NSF/SHINE (ATM 0204588). NG thanks the organizers of the ISCS 2003 symposium for the invitation and partial travel support.

REFERENCES

Brueckner, G. E. et al., 1995, Solar Phys., 162, 357

Burkepile, J. T., St. Cyr, O. C., 1993, NCAR/TN-369+STR

Cliver, E. W., St. Cyr, O. C., Howard, R. A., McIntosh, P. S., 1994, in Solar Coronal Structures, ed. V. Rusin, P. Heinzel, and J.-C. Vial, VEDA Publishing Co., Bratislava, p. 83-89

Crooker, N. U., 2000, JASTP, 62, 1071.

Gopalswamy, N., 1999, in Solar Physics with Radio Observations, Eds.: T. S. Bastian, N. Gopalswamy and K. Shibasaki, NRO Report No. 479, p.141-152

Gopalswamy, N., Lara, A., Kaiser, M. L., Bougeret, J.-L., 2001a, JGR, 106, 25261

Gopalswamy, N., Yashiro, S., Kaiser, M. L., Howard, R. A., Bougeret, J.-L., 2001b, JGR, 106, 29219

Gopalswamy, N., 2002, in Solar Terrestrial Magnetic Activity and Space Environment, ed. H. N. Wang and R. L. Xu, CPSPAR Colloquia Ser., vol. 14, p. 157-164

Gopalswamy, N., 2003, Adv. Space Res., 31, no. 4, 869

Gopalswamy, N., Lara, A., Lepping, R. P., Kaiser, M. L., Berdichevsky, D., St. Cyr, O. C., 2000, GRL, 27, 145

Gopalswamy, N., Lara, A., Kaiser, M. L., Bougeret, J.-L., 2001a, JGR, 106, 25261

Gopalswamy, N., Yashiro, S., Kaiser, M. L., Howard, R. A., Bougeret, J.-L., 2001b, JGR, 106, 29219

Gopalswamy, N., Yashiro, S., Michałek, G., Kaiser, M. L., Howard, R. A., Reames, D. V., Leske, R., von Rosenvinge, T. 2002, ApJ, 572, L103

Gopalswamy, N., Yashiro, S., Nunes, S., Howard, R. A., 2003, Adv. Space Res. in press, 2003a

Gopalswamy, N., Shimojo, M., Lu, W., Yashiro, S., Shibasaki, K., Howard, R. A., 2003b, ApJ, 586, 562

Gopalswamy, N., Yashiro, S., Lara, A., Kaiser, M. L., Thompson, B. J., Gallagher, P. T., Howard, R. A., 2003c, GRL, 30, 3

Hoeksema, J. T., 1992, in Solar Wind Seven, eds. E. Marsch, R. Schwenn, Pergamon, New York, p. 191-196

Hildner, E., Gosling, J. T., MacQueen, R. M., Munro, R. H., Poland, A. I., Ross, C. L., 1976, Solar Phys., 48, 127

Howard, R. A., Michels, D. J., Sheeley, N. R., Koomen, M. J., 1982, ApJ 263, L101

Hundhausen, A., 1999, in The many faces of the sun: a summary of the results from NASA's Solar Maximum Mission., eds. K. T. Strong, J. L. R. Saba, B. M. Haisch, J. T. Schmelz, p. 143

Ivanov, E. V., Obridko, V. N., 2001, Solar Phys., 198, 179

Lara, A., Gopalswamy, N., Nunes, S., Muñoz, G., Yashiro, S., 2003, GRL 30, 4

Lorenc, M., Pastorek, L., Rybansky, M., 2003, this volume

Low, B. C., 2001, JGR, 106, 25141

McIntosh, P. S., 2002, American Astronomical Society Meeting, 200, #57.03

Sheeley, N. R., Hakala, W. N., Wang, Y.-M., 2000, JGR, 105, 5081

St. Cyr, O. C., Burkepile, J. T., Hundhausen, A. J., Lecinski, A. R., 1999, JGR, 104, 12493

St Cyr, O.C. et al., 2000, JGR, 105, 18169

Tousey, R., Howard, R. A., and Koomen, M. J., 1974, Bull. American Astron. Soc., 6, 295

Webb, D. F., 2002, in Half a Solar Cycle with SOHO, ed. A. Wilson, ESA SP-508, Noordwijk: ESA Publications, p. 409 - 419

Webb, D. F., Howard, R. A., 1994, JGR, 99, 4201

Webb, D. F., Cliver, E. W., Crooker, N. U., St. Cyr, O. C., Thompson, B. J., 2000, JGR, 105, 7491